5-29-2015

Magnetic Structure and Ordering of Multiferroic Hexagonal $LuFeO_3$

Daniel A. Hillsberry
Boise State University

Eric L. Thies
Boise State University

Dmitri A. Tenne
Boise State University

Publication Information

Hillsberry, Daniel A.; Thies, Eric L.; and Tenne, Dmitri A. (2015). "Magnetic Structure and Ordering of Multiferroic Hexagonal $LuFeO_3$". *Physical Review Letters, 114*(21), 217602-1 - 217602-6. http://dx.doi.org/10.1103/PhysRevLett.114.217602

Magnetic Structure and Ordering of Multiferroic Hexagonal $LuFeO_3$

Steven M. Disseler
NIST Center for Neutron Research
National Institute of Standards and Technology
Gaithersburg, Maryland

Julie A. Borchers
NIST Center for Neutron Research
National Institute of Standards and Technology
Gaithersburg, Maryland

Charles M. Brooks
Department of Materials Science and Engineering
Cornell University
Ithaca, New York

Julia A. Mundy
School of Applied and Engineering Physics
Cornell University
Ithaca, New York

Jarrett A. Moyer
Department of Physics and Frederick Seitz Materials Research Laboratory
University of Illinois at Urbana-Champaign
Urbana, Illinois

D. A. Hillsberry
Department of Physics
Boise State University
Boise, Idaho

E. L. Thies
Department of Physics
Boise State University
Boise, Idaho

D. A. Tenne
Department of Physics
Boise State University
Boise, Idaho

John Heron
Department of Materials Science and Engineering
Cornell University
Ithaca, New York

Megan Holtz
School of Applied and Engineering Physics
Cornell University
Ithaca, New York

James D. Clarkson
Department of Materials Science and Engineering
University of California
Berkeley, California

Gregory M. Stiehl
Department of Physics
Cornell University
Ithaca, New York

Peter Schiffer
Department of Physics and Frederick Seitz Materials Research Laboratory
University of Illinois at Urbana-Champaign
Urbana, Illinois

David A. Muller
School of Applied and Engineering Physics
Cornell University
Ithaca, New York

and

Kavli Institute at Cornell for Nanoscale Science
Ithaca, New York

Darrell G. Schlom
Department of Materials Science and Engineering
Cornell University
Ithaca, New York

and

Kavli Institute at Cornell for Nanoscale Science
Ithaca, New York

William D. Ratcliff
NIST Center for Neutron Research
National Institute of Standards and Technology
Gaithersburg, Maryland

Abstract

We report on the magnetic structure and ordering of hexagonal $LuFeO_3$ films of variable thickness grown by molecular-beam epitaxy (MBE) on YSZ (111) and Al_2O_3 (0001) substrates. These crystalline films exhibit long-range structural uniformity dominated by the polar $P6_3cm$ phase, which is responsible for the paraelectric to ferroelectric transition that occurs above 1000 K. Using bulk magnetometry and neutron diffraction, we find that the system orders into a ferromagnetically-canted antiferromagnetic state via a single transition below 155 K regardless of film thickness, which is substantially lower than that previously reported in hexagonal $LuFeO_3$ films. The symmetry of the magnetic structure in the ferroelectric state implies that this material is a strong candidate for linear magnetoelectric coupling and control of the ferromagnetic moment directly by an electric field.

Multiferroic materials display both ferroelectric and magnetic order and have been the subject of intense investigation both from fundamental and applied perspectives [1, 2]. For example, if both order parameters are coupled, these materials would enable new devices ranging from magnetic field sensors to magnetic random access memory. Unfortunately, single-phase multiferroics are extraordinarily rare; thus far only four room temperature single-phase multiferroics have been reported: $BiFeO_3$ [3], $BiCoO_3$ [4], $ScFeO_3$ with the corundum structure [5], and most recently hexagonal $LuFeO_3$ (*h*-$LuFeO_3$) [6]. The latter compound, *h*-$LuFeO_3$ was found to be isostructural with $YMnO_3$ (Fig. 1(a)) [7, 8] when synthesized in thin film form, and antiferromagnetism appears to persist in the ferroelectric state well above room temperature. Our current investigation of the same system reveals that hexagonal $LuFeO_3$ is a multiferroic, but the onset of magnetic order is well below room temperature.

Specifically, $YMnO_3$ and other hexagonal manganites, $REMnO_3$ (RE=Lu, Y, Ho), have been known for some time to exhibit multiferroic properties. The ferroelectric transition in these materials is the result of a structural transition from the non-polar $P6_3/mmc$ to the polar $P6_3cm$ space group well above room temperature ($T_C \sim 900$ K in $YMnO_3$) [9]. Magnetic order sets in at much lower temperatures ($T_N \sim 80$ K in $YMnO_3$) [10], which renders these materials unsuitable for multiferroic device applications. Even in the magnetically ordered state at cryogenic temperatures, the coupling between the ferroelectric and magnetic order parameters is weak [11]. Replacing Mn with Fe in this system has been proposed as one way to increase both the magnetic transition temperature as well as the coupling between the two order parameters [12], and has been the subject of increased interest as of late [6, 13]. For example, theoretical calculations using first-principles suggest that a weak ferromagnetic moment along the *c*-axis may be deterministically switchable by 180° with an electric field [12].

Reports of antiferromagnetic order above room temperature in *h*-$LuFeO_3$ [6] coupled with theoretical predictions of a weak canted moment along the *c*-axis [12], which is observed at temperatures below 147 K [13], have generated significant interest in this material for device applications. In this Letter, we determine through magnetometry and neutron diffraction measurements the intrinsic magnetic structure of *h*-$LuFeO_3$ epitaxial films, which exhibit uniform $P6_3cm$ structural order. We find that antiferromagnetic order is evident as previously reported [6] but occurs only below 155 K for *h*-$LuFeO_3$ films of variable thickness on several substrates (i.e., Al_2O_3 and cubic zirconia). Furthermore, its onset occurs simultaneously with the onset of the weak ferromagnetic canting of the moments. From Raman scattering we demonstrate that *h*-$LuFeO_3$ is ferroelectric at room temperature, with a paraelectric-to-ferroelectric transition temperature $T_C = 1020$ K ± 50 K. Solving the magnetic structure we confirm that the films magnetically order in the ferroelectric state in a manner that is completely consistent with theoretical predictions for the magnetoelectric effect such that electric field-induced reversal of the ferromagnetic moment direction should be achievable in this material below the magnetic ordering temperature (< 155 K). Our results thus contrast with previous reports of room temperature antiferromagnetic ordering in comparable *h*-$LuFeO_3$ films [6]. Subtle, but significant, deviations of the structure from the $P6_3cm$ phase in the films of the previous study are key to interpreting these differences in magnetic ordering temperatures.

We used oxide molecular-beam epitaxy (MBE) to grow six high quality, single-crystalline films of *h*-$LuFeO_3$ with thicknesses from 20 nm to 250 nm grown on 10 mm × 10 mm substrates of either (111)-oriented yttria-stabilized cubic zirconia (YSZ) or (0001) Al_2O_3 [13]. MBE affords greater control over synthesis parameters resulting in lower

disorder, higher quality films than other oxide-growth techniques such as PLD [14]. The list of samples is provided in Table 1. For simplicity, each sample considered in this work will be designated by their substrate and $LuFeO_3$ thickness (e.g., YSZ-200 nm).

In Fig. 1(b), we show as an example a θ-2θ XRD scans for YSZ-250 nm. The intense narrow peaks come from the substrate, while the other reflections come from the film and demonstrate that it is single phase. Only 00*l* reflections with even *l* are observed indicating the (001) orientation of the film and consistent with the $P6_3cm$ space group as shown in Fig. 1(a). Similar patterns are observed for the remaining samples [15]. From STEM images along the [110] zone axis of *h*-$LuFeO_3$ shown in Fig. 1(c), the interface between the film and substrate is seen to be abrupt and free of impurity phases. This film is also nearly free of extra Fe-O layers (syntactic intergrowths of $LuFe_2O_4$) [13], which are occasionally observed in similar films [15]. TEM images reveal that the Lu atoms in each plane are displaced in an "up down down" pattern over extended length scales, consistent with the noncentrosymmetric, polar $P6_3cm$ structural phase. While TEM images [Fig. S2, Ref. 6] from previous investigations of related *h*-$LuFeO_3$ films show local regions with the Lu atoms in the "up down down" pattern, these areas are interspersed within larger regions that exhibit a "up middle down" pattern. The latter arrangement is consistent with closely related structural phases such as antipolar *P-3c* that appears to be intermixed with the polar $P6_3cm$ structural phase.

The lattice parameters for each sample in the current study were obtained from neutron diffraction measurements of the 300 and 004 nuclear reflections at 5 K as shown in Table 1. These values appear to be independent of both sample thickness and substrate and are within error of previously reported values for stoichiometric films [6, 13]. Films with thicknesses 200 nm or greater exhibit resolution-limited peak shapes at nuclear reflections [15] indicating no distribution of lattice parameters for strain or finite-size effects, while films of 20 nm and 70 nm are broadened only along 00*l* in accordance with reduced physical dimensions along that direction. Based on these results, it does not appear that the strain potentially induced by the substrate-film interface plays any significant role in determining the overall crystallographic, ferroelectric, or magnetic properties of this system regardless of film thickness.

Raman measurements, shown for YSZ-200 nm in Fig. 2, reveal that the ferroelectric transition occurs well above room temperature. The observed peak positions in the Raman spectra and relative intensities are very similar to that of hexagonal $LuMnO_3$ [16] as opposed to those reported for bulk orthorhombic $LuFeO_3$ [17]; the spectra correspond to that of *h*-$LuFeO_3$. We are able to distinguish at least 10 phonon modes out of the 23 that are active in the scattering geometries used, consistent with its ferroelectric structure [15]. The temperature dependence of the integrated Raman intensity of the strongest A_1 peak, near 655 cm^{-1} [normalized by the Bose factor $n + 1 = 1/(1 - e^{-\hbar\omega/kT})$] is shown in the inset. The intensity decreases linearly with increasing temperature between 400 K and 1000 K, above which no change is observed; a linear fit of the intensity over this temperature region demonstrates a clear transition to a non-polar phase at T_c = 1020 K ± 50 K. Piezoelectric force microscopy measurements have shown switching of the ferroelectric polarization in these films [15], consistent with ferroelectricity above room temperature similar to the hexagonal manganites, and confirm previous reports [6, 8].

As expected from theory [12], bulk magnetization measurements indicate that the onset of ferromagnetic order is not coincident with the ferroelectric transition, instead occurring well below room temperature. Measurements of the magnetization along the *c*-axis of YSZ-250 nm are shown in Fig. 1(d). A clear transition can be seen in the field-cooled data at 143 K. While the magnitude of the magnetization is small ($\sim 0.02\mu_B$), it is clear evidence for weak ferromagnetism occurring in the ordered phase. The presence of weak ferromagnetism is common among all samples in this study, with onset temperatures between 118 K and 150 K [14]. The offset between FC and ZFC at higher temperatures in some samples is indicative of trace amounts of Fe_3O_4 or similar impurity phase that occurs in conjunction with syntactic intergrowths seen in TEM [15]. Beyond this, we find no evidence for additional magnetic transitions at or above room temperature in measurements of the magnetic susceptibility, as shown in the inset of Fig. 1(d). Similar susceptibilities have been measured for magnetic fields applied parallel to the plane of the film indicating isotropic magnetic susceptibility above room temperature, in contrast to the previous report [6].

We now turn our focus to the magnetic neutron diffraction results, which provide a full picture of the corresponding antiferromagnetic order. We measured the temperature dependence (Fig. 3) of several reflections including the 101, 100, and 102, which are predominantly (or entirely) of magnetic origin. Interpretation of the differences among the temperature dependence of these reflections, however, first requires an understanding of the possible **q**=0 magnetic structures consistent with the $P6_3cm$ space group. Representational analysis reveals that the magnetic and crystallographic unit cells of these materials are identical (**q**=0) and that the magnetic structure of these materials may

fall into six representations: four one-dimensional and two two-dimensional [18-20]. For the hexagonal manganites, the materials measured thus far have been well described by the one-dimensional representations which contain the classic 120° arrangement of spins in a given plane, labeled as Γ_1 to Γ_4 as shown in Figs. 4(a)-4(d), respectively. Planes can either be coupled ferromagnetically (Γ_3 and Γ_4) or antiferromagnetically (Γ_1 and Γ_2) along the *c*-axis, and the moments may lie along the *a* or *b* crystallographic axes with respect to the 120° arrangement of the spins. Furthermore, only the Γ_2 representation allows for a net moment to develop along the *c*-axis. Unfortunately, the Fe atoms lie at the $(\frac{1}{3}00)$ position, such that the Γ_1 and Γ_3 representations form a homometric pair, as do the Γ_2 and Γ_4 representations. Members of the same homometric pair cannot be distinguished by unpolarized neutron scattering [19]. Different homometries may still be distinguished through unpolarized diffraction by the presence of the 100 magnetic reflection which is found only for the Γ_1 and Γ_3 representations.

In Fig. 3 (a-f) we show detailed neutron diffraction results for YSZ-200 nm and Al_2O_3-200 nm as examples, noting that similar measurements were made on all six individual films [15]. The 101 reflection is present at low temperatures for all films grown on both YSZ and Al_2O_3 substrates, including films with thicknesses of only 70 nm and 20 nm as shown in Figs. 3(g) and 3(h) respectively, and clearly absent above the transition temperature determined by magnetometry. Our measurements show no evidence of magnetic scattering above 155 K regardless of thickness, as demonstrated in Fig. 3(i) in which the temperature dependence of the normalized intensity of the this reflection is shown for films fabricated on Al_2O_3 with thicknesses ranging from 20 nm to 250 nm.

The temperature dependence of the scattering intensity of several magnetic reflections measured on warming is shown in Figs. 3(c) and 3(f). The antiferromagnetic ordering temperature T_N is determined by fitting the 101 and 102 reflections with a mean-field order parameter, from which we find 115(20) K < T_N < 155(5) K for all samples listed in Table 1. These values agree quite well with the onset of ferromagnetism obtained from magnetometry, indicating that both in-plane magnetic order and canted moments develop simultaneously and only well below room temperature in these stoichiometric *h*-$LuFeO_3$ films.

These results directly contradict the interpretation of the temperature dependence of the 102 reflection in a stack of 20 nm films, as detailed in the previous report [6]. The expected peak intensities of the 102 reflection is extremely sensitive to the precise symmetry of the structural phase. For example, relative to that expected for the polar $P6_3cm$ phase, the structural contribution to the 102 intensity is larger for the non-polar, centrosymmetric *P*-3*c* phase (which is consistent with the arrangement of the Lu atoms in the TEM images for their samples [6]) and smaller for the $P6_3mmc$, and $P6_3mcm$ phases. It is thus plausible that the apparent transition reported in Ref. 6 is not magnetic in nature, but rather represents a structural transition near or just above room temperature. As in that study many films were coaligned, only a small fraction of the structure in any particular film would have to transform to give rise to a substantial change in the 102 peak intensity.

Significant intensity is also observed at the 100 reflection for the films in Ref. 6 though it vanishes near 130 K, which is roughly consistent with T_N for the films in our current study. Several of our films also have temperature-dependent 100 scattering (Figs. 3(b) and 3(e)), though, it is apparent that this reflection does not appear simultaneously with the 101 and 102 magnetic reflections. Rather, the appearance of the 100 reflection is consistent with a reorientation of the moments within the *hk*0 plane below T_N, which has been observed in similar systems [20]. The reorientation temperature, T_R, is again determined from a fit of a mean-field order parameter of the 100 scattering intensity, from which we find T_R = 53 ± 3 K (YSZ-250 nm) and 38 ± 3 (Al_2O_3-200 nm), while no such reorientation is discernable for YSZ-200 nm or Al_2O_3-250 nm [15]. For YSZ-250 nm and Al_2O_3-200 nm, the ground state magnetic structure can be described by a combination of the $\Gamma_1+\Gamma_2$ representations as shown in Fig. 4(e), and is consistent with that suggested based on previous measurements [6], while a single Γ_2 representation alone is adequate to describe Al_2O_3-250 nm. From the relative intensities of the 100 and 101 reflections we find this effect is quite small, with a maximum possible rotation of only 15° in plane and with no effect on the ferromagnetic moment we observe. Determination of the structural origin of the variation (or absence) of T_R in our samples would require a precise crystallographic refinement of the Fe position and distortion of the O bipryamid [21, 22] that is not feasible due to the geometric characteristics of these epitaxial thin films.

As no spin reorientation was observed in Al_2O_3-250 nm, we may more easily refine the magnetic structure including the magnitude of the ordered Fe moments at 5 K from the integrated intensities of several magnetic and structural peaks. These intensities have been corrected to account for the resolution function and appropriately scaled by the

intensities of the 004 and 300 nuclear peaks to obtain the proper structure factors listed in Table 2. The magnetic structure is refined using the Γ_2 representation with the out-of-plane component of the moments fixed to zero, as these magnetic reflections are insensitive to the canted moment. The refinement is in excellent agreement with the data, from which we extract an ordered magnetic moment of 2.9(5) μ_B /Fe. The moment is reduced from that expected for the $S = 5/2$ Fe^{3+}, but follows similar observations of reduced moments in hexagonal manganites [18, 19]. While this refinement was performed using only a single magnetic domain, it should be noted that including equal populations of magnetic domains as discussed in Ref. [12] produces a statistically similar refinement of the data, and with a comparable magnetic moment on the Fe site.

We conclude that uniform films with variable thickness of metastable *h*-$LuFeO_3$ can be stabilized on different substrates. Our films exhibit robust canted antiferromagnetic order below 155 K, which is substantially below the value (440 K) previously reported [6]. Furthermore, we have demonstrated that the magnetic structure in the ordered state of *h*-$LuFeO_3$ does not depend strongly on the underlying substrate or film thickness and that the canting and Neel state appear as a single transition; the differences (in T_N, for example) that do occur among our samples cannot be attributed to differences in strain. The universal appearance of a ferromagnetically-canted antiferromagnet in the ferroelectric state indicates that the films contain the proper symmetries in the ordered state to support coupling of the ferromagnetic moment directly to an electric field as theoretically proposed [12]. In future work, it will prove interesting to determine whether this observed canted magnetic moment is indeed switchable with electric field, since the films are ferroelectric at temperatures well above room temperature. If so, then further efforts will be warranted to determine if it is possible to increase the magnetic transition temperature in this system, or whether the lessons we learn from this material can be applied in the hunt for materials with similar magnetic properties, but with higher transition temperatures.

Acknowledgements

The authors would like to thank Hena Das, Craig Fennie, Jeffrey Lynn, Leland Harrigner and Daniel Parshall for helpful discussions. Research supported by the U.S. Department of Energy, Office of Basic Energy Sciences, Division of Materials Sciences and Engineering, under Award No. DE-SC0002334. This work made use of the electron microscopy facility of the Cornell Center for Materials Research with support from the National Science Foundation (NSF) Materials Research Science and Engineering Centers program (DMR 1120296) and NSF IMR0417392. This work was performed in part at the Cornell NanoScale Facility, a member of the National Nanotechnology Infrastructure Network, which is supported by the National Science Foundation (Grant ECCS-0335765). Raman studies at Boise State University have been supported by NSF under grant DMR-1006136, and by M. J. Murdock Charitable Trust “Partners in Science” program (E. L. T.).

References

[1] S.-W. Cheong and M. Mostovoy, Nat. Mater. **6**, 14 (2007).

[2] R. Ramesh and Niola A. Spaldin, Nat. Mater. **6**, 21 (2007).

[3] J. Wang, J. B. Neaton, H. Zheng, V. Nagarajan, S. B. Ogale, B. Liu, D. Viehland, V. Vaithyanathan, D. G. Schlom, U. V. Waghmare, N. A. Spaldin, K. M. Rabe, M. Wuttig, and R. Ramesh, Science **299**, 1719 (2003).

[4] A. A. Belik, S. Iikubo, K. Kodama, N. Igawa, S. Shamoto, S. Niitaka, M. Azuma, Y. Shimakawa, M. Takano, F. Izumi, and E. Takayama-Muromachi, Chem. Mater. **18**, 798 (2006).

[5] M. R. Li, U. Adem, S. R. C. McMitchell, Z. Xu, C. I. Thomas, J. E. Warren, D. V. Giap, H. Niu, X. Wan, R. G. Palgrave, F. Schiffmann, F. Cora, B. Slater, T, L. Burnett, M. G. Cain, A. M. Abakumov, G. Tendeloo, M. F. Thomas, M. J. Rosseinsky, and J. B. Claridge, J. Am. Chem. Soc. **134**, 3737 (2012).

[6] W. Wang, J. Zhao, W. Wang, Z. Gai, N. Balke, M. Chi, H. N. Lee, W. Tian, L. Zhu, X. Cheng, D. J. Keavney, J. Yi, T. Z. Ward, P. C. Snijders, H. M. Christen, W. Wu, J. Shen, and X. Xu, Phys. Rev. Lett. **110**, 237601 (2013).

[7] A. A. Bossak, I. E. Graboy, O. Y. Gorbenko, A. R. Kaul, M. S. Kartavtseva, V. L. Svetchnikov, and H. W. Zandbergen, Chem. Mater. **16**, 1751 (2004).

[8] Y. K. Jeong, J.-H. Lee, S.-J. Ahn, H. M. Jang, Chem. Matter. **24** 2426 (2012).

[9] G. A. Smolenskii and V. A. Bokov, J. Appl. Phys. **35**, 915 (1964).

[10] T. Katsufuji, S. Mori, M. Masaki, Y. Moritomo, N. Yamamoto, and H. Takagi, Phys. Rev. B **64**, 104419 (2001).

[11] B. B. Van Aken, T. T. M. Palstra, A. Filippetti, and N. A. Spaldin, Nat. Mater. **3**, 164 (2004).

[12] H. Das, A. L. Wysocki, Y. Geng, W. Wu, and C. J. Fennie, Nat. Commun. **5**, 2998 (2014).

[13] J. A. Moyer, R. Misra, J. A. Mundy, C. M. Brooks, J. T. Heron, D. A. Muller, D. G. Schlom, and P. Schiffer, APL Mater. **2**, 012106 (2014).

[14] Tsuyoshi Ohnishi, Keisuke Shibuya, Takahisa Yamamoto, and Mikk Lippmaa, J. Appl. Phys. **103**, 103703 (2008). Supplemental Information (*url*).

[15] A. Ghosh, J. R. Sahu, S. V. Bhat, and C. N. R. Rao, Solid State Sci. **11**, 1639 (2009).

[16] S. Venugopalan and M. M. Becker, J. Chem. Phys. **93**, 3833 (1990).

[17] S. Quezel, J. Rossat-Mignod, and E. F. Bertaut, Solid State Commun. **14**, 941 (1974).

[18] P. J. Brown and T. Chatterji, J. Phys.: Condens. Matter **18**, 10085 (2006).

[19] A. Munoz, J. A. Alonso, M. J. Martinez-Lopez, M. T. Casais, J. T. Martinez, and M. T. Fernandez-Diaz. Phys. Rev. B **62**, 9498 (2000).

[20] H. Wang, I. V. Solovyev, W. Wang, X. Wang, P. J. Ryan, D. J. Keavney, J-W. Kim, T. Z. Ward, L. Zhu, J. Shen, X. M. Cheng, L. He, X. Xu, and X. Wu, Phys. Rev. B **40**, 014436 (2014).

[21] X. Fabre`ges, S. Petit, I. Mirebeau, S. Pailhe`s, L. Pinsard, A. Forget, M. T. Fernandez-Diaz, and F. Porcher, Phys Rev. Lett. **103**, 067204 (2009).

Table 1. Lattice parameters for each sample from measurements of the nuclear 300 and 004 reflections below 10 K and Neel temperature obtained from the best fit-mean-field order parameter. Errors in parenthesis represent one standard deviation of the last digit as obtained from least-squares fitting.

Sample	***a* (Å)**	***c* (Å)**	T_N
200 nm on YSZ	5.989(5)	11.70(3)	155(5) K
250 nm on YSZ	5.979(5)	11.81(3)	150(1) K
200 nm on Al_2O_3	5.985(5)	11.77(2)	140(2) K
250 nm on Al_2O_3	5.994(5)	11.78(2)	139(1) K
70 nm on Al_2O_3	6.05(3)	11.97(5)	115(20) K
20 nm on Al_2O_3	6.015(10)	11.84(5)	130(15) K

Table 2. Refinement of the magnetic structure factors measured from integrated intensities at 5 K for Al_2O_3-250 nm. The statistical agreement is given by $\chi^2 = 1.6$.

Reflection	F_{calc2}	F_{obs2}
100	0	0.01(2)
101	4.9	4.7(3)
102	2.0	2.7(4)
201	3.1	2.9(4)

Figure Captions

FIG. 1 (Color Online) Characterization of a 250 nm thick film of *h*-$LuFeO_3$ on YSZ (YSZ-250 nm). (a) Schematic of the crystal structure of *h*-$LuFeO_3$ with the $P6_3cm$ space group. (b) XRD at room temperature, with *h*-$LuFeO_3$ 00*l* reflections labeled accordingly; substrate peaks are denoted by (*). (c) STEM image of the film near the interface between *h*-$LuFeO_3$ and the substrate. (d) Magnetization under FC (closed circles) and ZFC (open circles) conditions. Inset: high temperature magnetization for magnetic fields 0.01 T, 0.05 T, and 0.1 T applied parallel to the *c*-axis.

FIG. 2 (Color Online) Raman spectra of 200 nm thick *h*-$LuFeO_3$ (YSZ-200 nm) measured at 10 K using both polarizations [15], demonstrating the Raman active phonon modes in the ferroelectric state of *h*-$LuFeO_3$. Inset: Normalized Raman intensity of the A_1 mode (peak around 650 cm^{-1}) as a function of temperature. The red line is a linear fit over the temperature region 400 K < T < 1050 K.

FIG. 3 (Color Online) Determination of the antiferromagnetic structure using neutron diffraction. The scattered intensity of the magnetic 101 and 100 reflections above and below T_N and temperature dependence for the (a-c) YSZ-250 nm and (d-f) Al_2O_3-200 nm. (g-h) Intensity of the 101 reflection Al_2O_3-70 nm and Al_2O_3-20 nm respectively. (i) The temperature dependent intensity of the 101 reflection for all four film thicknesses deposited on Al_2O_3. Solid lines in (c), (f), and (i) represent best fits of the data with a mean-field order parameter function, while lines in remaining figures are Gaussians.

FIG. 4. (a)-(d) Illustration of the four possible one-dimensional representations for *h*-$LuFeO_3$. The possible magnetic structures below T_R consisting of a combination of representations in (a)-(d) are shown in (e) and (f). Labels in parenthesis refer to the equivalent notation used in Ref. [12], for example.

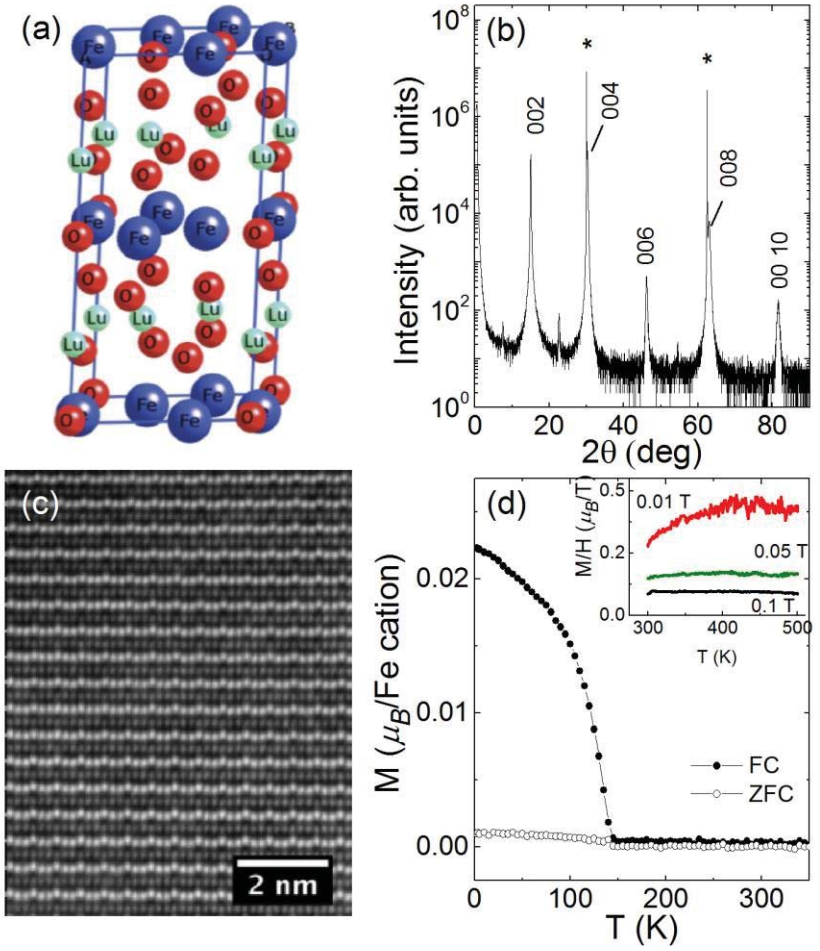

FIG. 1.

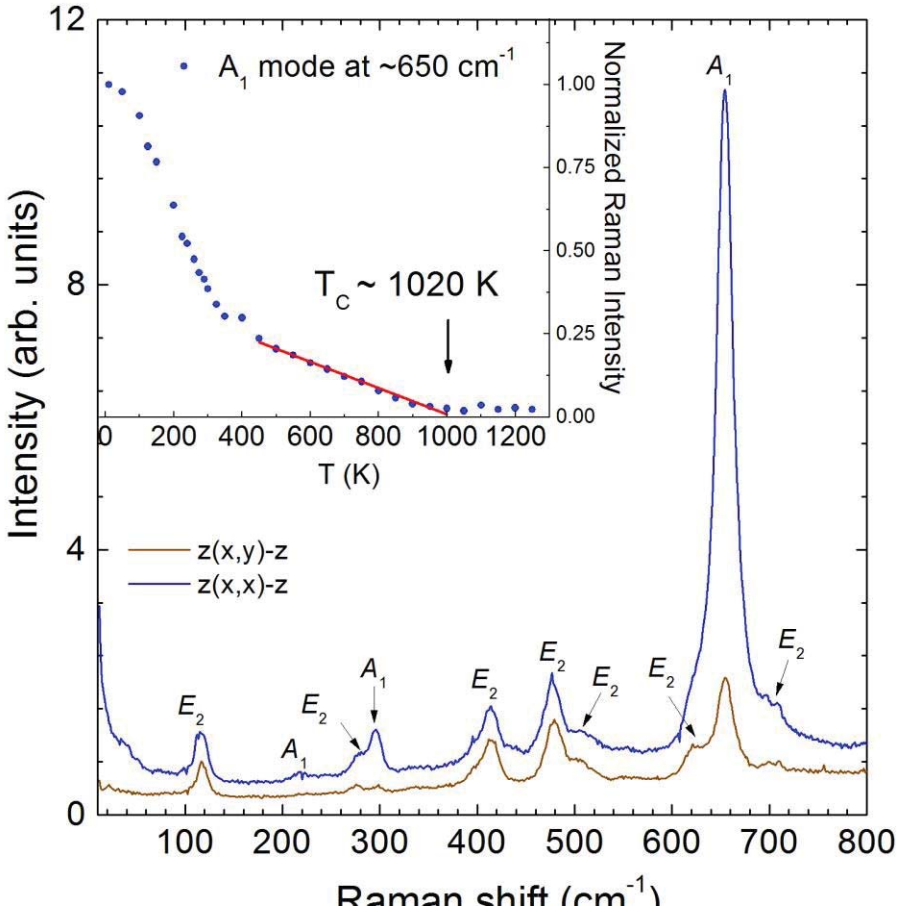

Fig. 2

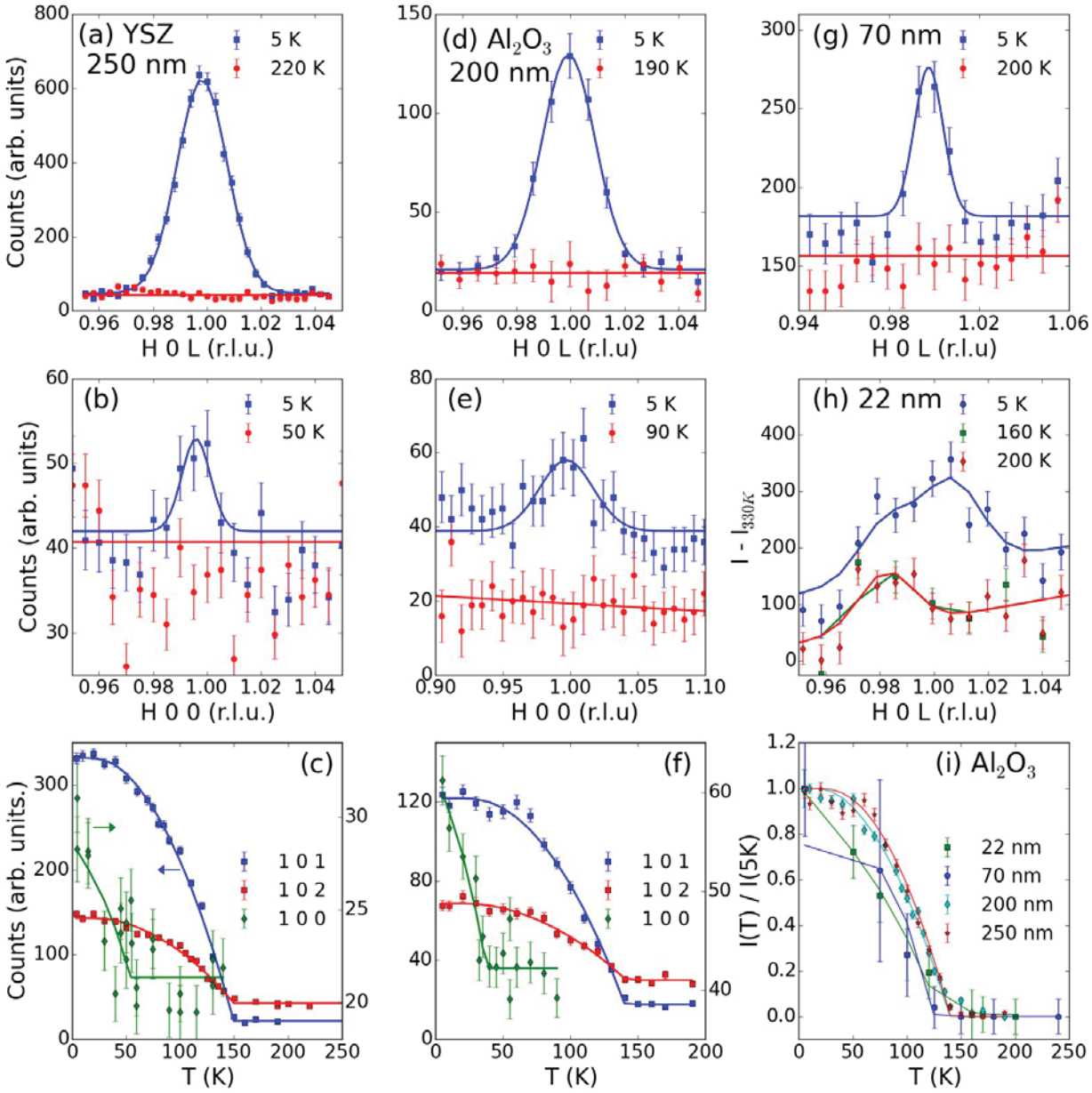

FIG. 3.

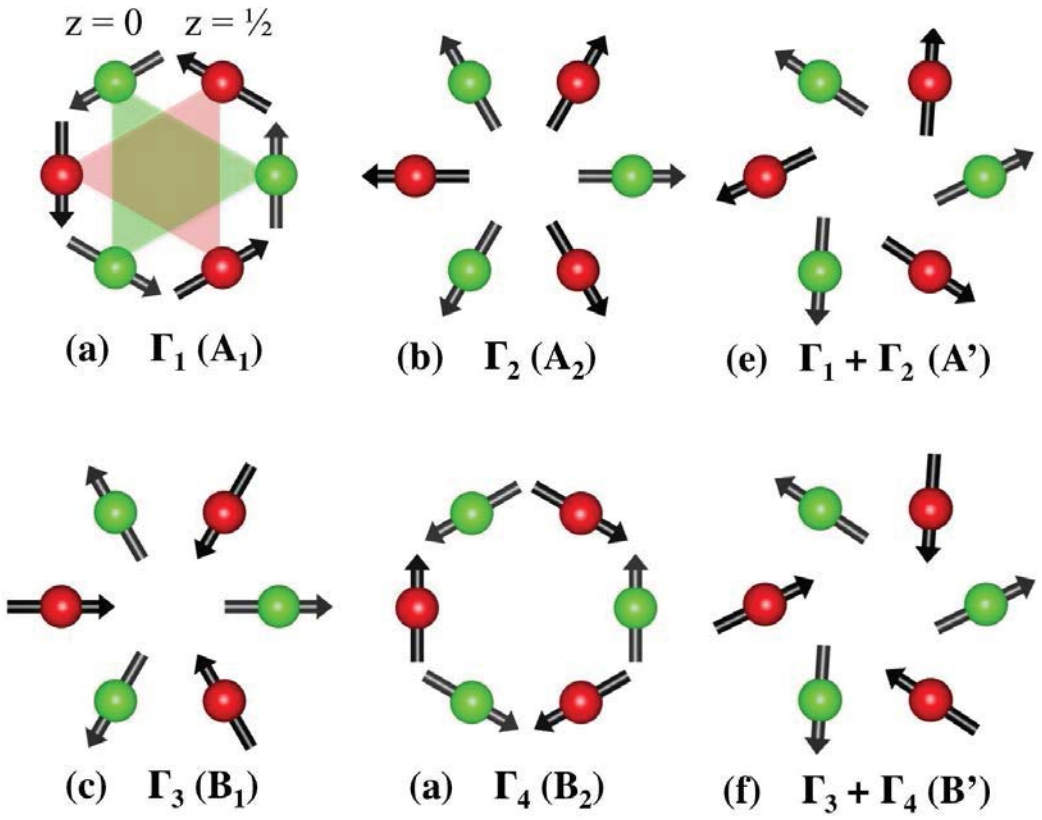

FIG. 4.

Supplemental Information

Measurement Details and Characterization of *h*-$LuFeO_3$ Films

High-resolution X-ray diffraction (XRD) using a four-circle diffractometer along with high-angle annular dark field scanning transmission electron microscopy (HAADF-STEM) were used to characterize the microstructure and assess the quality of the films. The magnetic moment along the *h*-$LuFeO_3$ *c*-axis was measured with a SQUID magnetometer upon warming in a small field (0.01 T) after first cooling in either zero field (ZFC) or in an out-of-plane field of 0.1 T (FC). Raman spectroscopy was performed on a single sample, YSZ-200 nm, between 10 K and 1250 K. Neutron diffraction experiments were performed on the BT-4 thermal triple axis at the NIST Center for Neutron Research to determine the magnetic structure and to further characterize the temperature dependence of the magnetization. For neutron diffraction, individual films were measured separately to reduce errors arising from the stacking of many such films together and to reduce the effect of inhomogeneities in films fabricated at different times.

STEM analysis was also performed on a 200 nm film grown on (0001) Al_2O_3, (Al_2O_3-200 nm) as shown in Fig. S1. The substrate-film interface is seen to be sharp, single phase, and free of double iron oxide layers (syntactic intergrowths of $LuFe_2O_4$). A general survey of the entire film thickness indicates the presence of such occasional intergrowths, as seen in the inset of Fig. S1(a). These are found to occur more frequently in this sample (Al_2O_3-200 nm) that in the sample grown on YSZ (YSZ-250 nm) shown in Fig. 1. A high-resolution image using Z-contrast HAADF-STEM is shown in Fig. S1(b) further demonstrating that the film is well-ordered and that the displacements of the Lu-ions are clearly "up, down, down" over large regions. In this image, all Lu-ions follow the same displacement pattern indicating that the ferroelectric domains is larger than the dimensions of the image, and that no antipolar or non-polar phases exist on this scale.

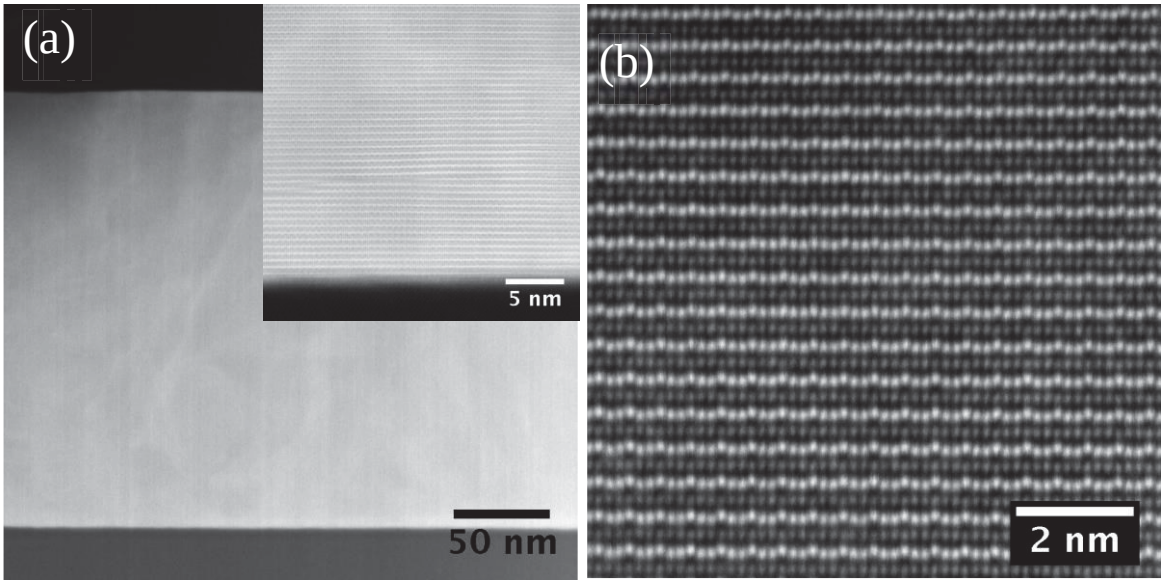

Fig. S1. STEM images of Al_2O_3-200 nm on Al_2O_3.

For XRD, a 220 Ge monochromator was place before the sample to select only Cu $_{K\alpha 1}$ radiation. Only the even 00*l* reflections are observed as shown in Fig. S2, therefore, films are oriented with the *c*-axis normal to the substrate surface regardless of substrate used. The lack of odd 00*l* reflections is consistent with the $P6_3cm$ structure. An enlarged view of the 004 reflection for films fabricated on YSZ shows there is no change in the *c*-lattice parameter within error between these films.

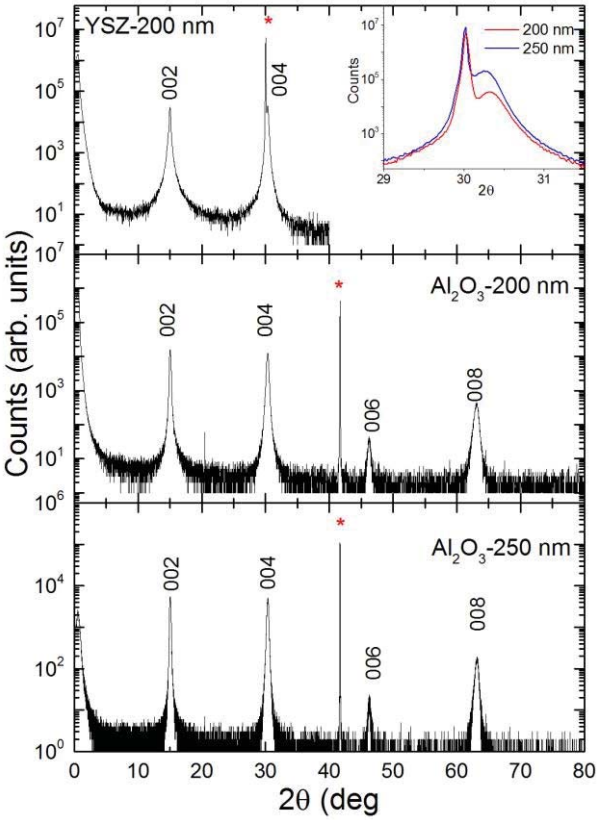

Fig. S2 XRD of YSZ-200 nm, Al_2O_3-200 nm and Al_2O_3-250 nm; 00*l* reflections are labeled accordingly while those arising from the substrate are labeled with an asterisk (*).

SQUID magnetometry was performed on all samples that were examined via neutron diffraction. The results are shown in Fig. S3. For measurements of samples fabricated on YSZ, a bare YSZ substrate was also measured to allow for the subtraction of paramagnetic and diamagnetic backgrounds. The magnetic signal from the Al_2O_3 substrate is sufficiently small that there was no need for this subtraction, however, in the case of the thinnest films shown in Fig. S3(a-b) a small contribution from paramagnetic impurities in the substrate is found at low temperatures. From the onset of the ferromagnetic moment, we find transition temperatures of 123 K, 118 K, 146 K, 145 K, 140 K, and 150 K for Al_2O_3-20 nm, Al_2O_3-70 nm Al_2O_3-200 nm and Al_2O_3-250 nm, YSZ-200 nm, and YSZ-250 nm respectively. All are above the transition reported from magnetometry in [1] and indicate the bulk of the films are very close to ideal stoichiometry [2].

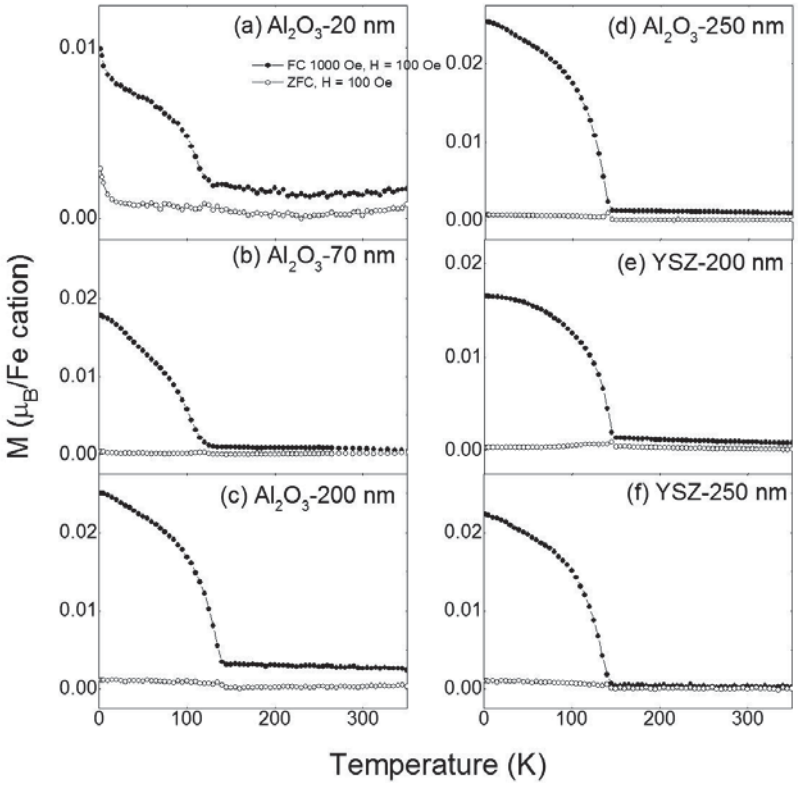

Fig. S3 Magnetic moment along the *c*-axis as a function of temperature for several samples fabricated on (a-d) Al_2O_3 and (e-f) YSZ. FC data is represented by closed circles and ZFC as open circles.

The field dependent magnetization was measured both above and below T_N as shown in Fig. S4 for the four thickest films. A background contribution that is constant above 200 K is observed in all samples, however the relative magnitude of this contribution is sample dependent and depends upon the relative portion of ferromagnetic inclusions within the bulk of the film [2].

There is a large opening of the hysteretic loop and increase in the saturation magnetization for all samples indicating a ferromagnetic ground state as suggested by the temperature dependence in Fig. S3 in addition to the antiferromagnetic order observed through neutron diffraction Together these confirm a ferromagnetically canted ground state for all samples of *h*-$LuFeO_3$ regardless of thickness or substrate.

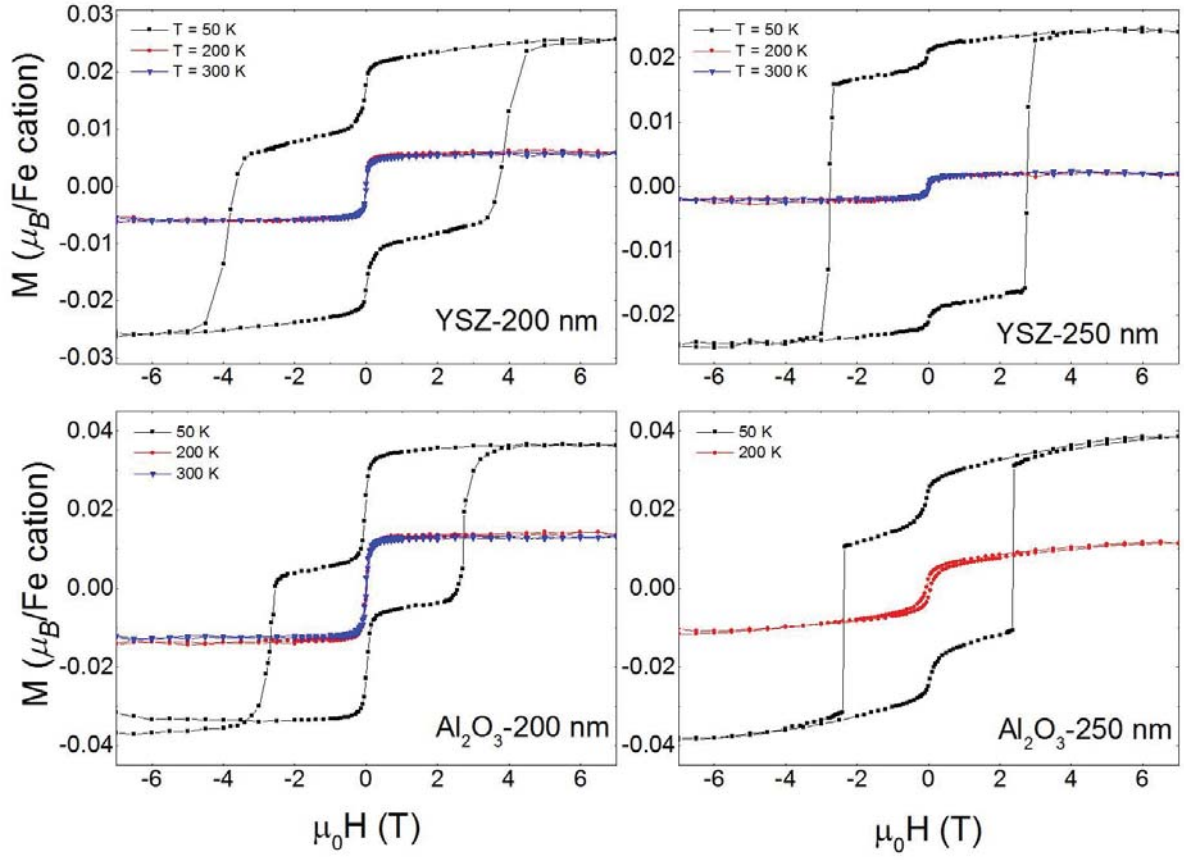

Fig. S4 Field dependent magnetization of YSZ-200 nm, YSZ-250 nm, Al_2O_3-200 nm and $Al_2O_3$250 nm samples with magnetic field applied parallel to the *c*-axis. The enlargement of the loops below 200 K is due to the ferromagnetic canting coinciding with T_N.

Neutron Diffraction and Strain Analysis

Pyrolitic Graphite (PG) filters were placed before and after the sample to remove $\frac{\lambda}{2}$ contamination from the beam. Both a monochromator (PG) and analyzer (PG) were employed to ensure elastic scattering (to within instrumental resolution). 40' collimators were employed before and after the monochromator as well as between the sample and the analyzer. Collimations were open between the analyzer and the detector. In the case of 70 nm and 20 nm films, no collimation was used prior to the monochromator to greatly increase the incident neutron flux. Order parameter measurements were performed with neutrons of incident energy E_i = 14.7 meV, while magnetic structure determination was performed with E_i = 35 meV. The sample was placed on a single crystal Si wafer to reduce background inside of an aluminum can sealed with He exchange gas to ensure thermal equilibration. Measurements were performed in a closed cycle refrigerator.

We determine the possibility of coherent strain in the lattice by examining the broadening of the nuclear peaks for both θ - 2θ as well as rocking curves with fixed 2θ for Al_2O_3-250 nm. In Fig. S5(b) and S5(d) we compare the measured θ - 2θ intensity with that calculated based the instrument collimations listed above and an ideal sample mosaic η_s, less than 30', normalized to the measured integrated intensity. These curves are in excellent agreement indicating the measurement is resolution limited such that there is no distribution of the lattice parameters along either the *a* or *c* directions. This suggests that the films are not coherently strained throughout the sample and that strain

between the substrate and the *h*-$LuFeO_3$ film is likely contained within a very narrow region. The in-plane sample mosaic, η_s, can then be approximated from the FWHM of the rocking curves shown in Fig. S5(a) and S5(c). The mosaic is found to have some directional dependence as η_s = 82' for the 004 reflection and η_s, = 67' for the 300 reflection.

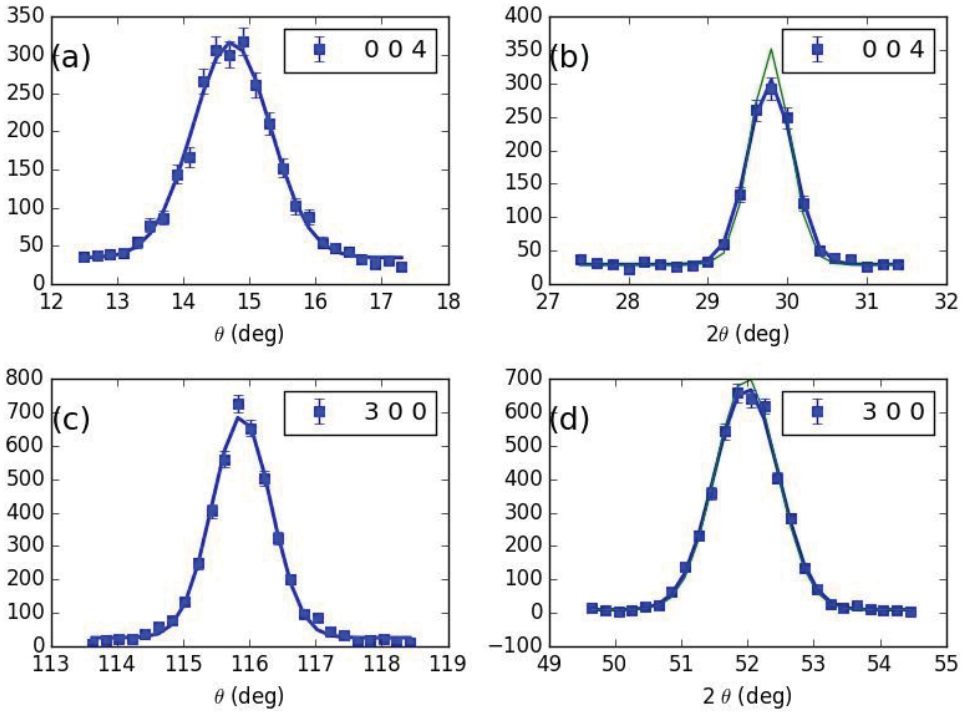

Fig. S5(a, c) Rocking (θ-scans) of the 004 and 300 reflections. (b, d) θ - 2θ scans of the same nuclear reflection, blue curves are fits to the data, while green curves are calculated based on known instrument resolution.

Magnetic Order Parameters

The intensity of the neutron diffraction of the 102 reflection, which is primarily magnetic in nature, was measured also measured for YSZ-200 nm shown in Fig. S6(a) at base and above room temperature. A well-defined peak is observed at base temperature, however, no intensity above background is observed at or above 300 K, which conclusively shows that no long-range magnetic order is present in this system at these temperatures. The magnetic ordering and reorientation temperature for YSZ-200 nm was determined by measuring the intensity of the 102 reflection as a function of temperature, shown in Fig. S6(b). The 100 was also measured, however no temperature dependence could be distinguished above background and noise. For Al_2O_3-250 nm, no 100 reflection was observed to 5 K, so only the 101 magnetic reflection was measured as shown in Fig. S6(c). The values of T_N were found to be 155 ± 5 K and 139 ± 1.5 K for YSZ-200 nm and Al_2O_3-250 nm, respectively.

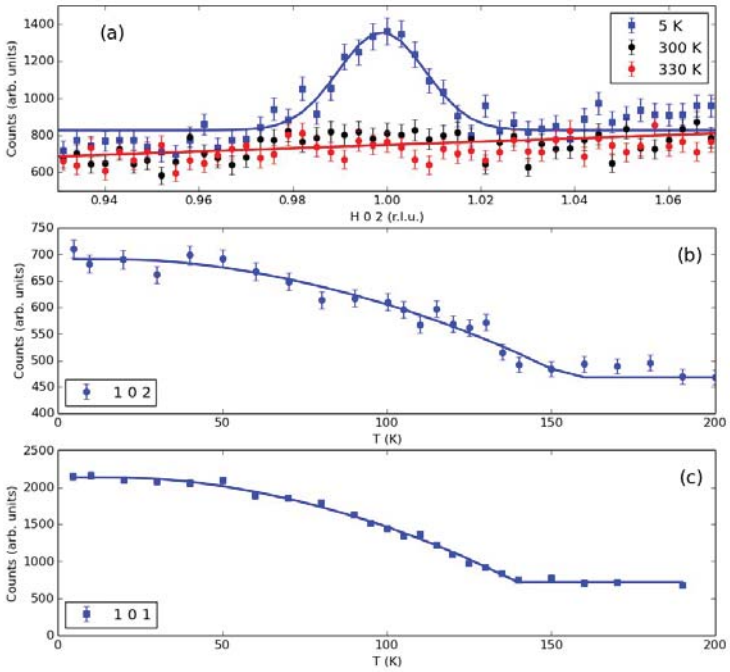

Fig. S6 (a) Transverse scans through the 102 reflection for YSZ-200 nm both near base temperatures and above room temperature. (b) Temperature dependent intensity of the 102 magnetic reflections for YSZ-200 nm, and (c) temperature dependence of the 101 magnetic reflection for Al_2O_3-250 nm.

Raman Scattering

Raman spectra of YSZ-200 nm, (a 200-nm thick *h*-$LuFeO_3$ film grown by MBE on a (111) YSZ substrates) were measured in backscattering geometry normal to the film surface using a triple spectrometer equipped with a liquid nitrogen cooled multichannel charge coupled device detector. An ultraviolet excitation (325 nm line of He-Cd laser) was used in order to reduce the substrate contribution. The substrate signal was completely suppressed with all signal arising from the $LuFeO_3$ film. Maximum laser power density was 0.5 W/mm^2 at the sample surface, low enough to avoid any noticeable local heating of the sample. Spectra for the $LuFeO_3$ sample were recorded in the temperature range 10–1250 K using a variable temperature closed cycle helium cryostat and a high-temperature stage.

Bulk unstrained $LuFeO_3$ has an orthorhombic (distorted perovskite) non-polar *Pbnm* structure (space group D_{2h}^{16}) with unit cell containing four formula units. A group theory analysis shows that the sixty phonon modes of orthorhombic $LuFeO_3$ belong to $7A_g + 5B_{1g} + 7B_{2g} + 5B_{3g} + 8A_u + 10B_{1u} + 8B_{2u} + 10B_{3u}$ symmetries [3]. Among these modes, one A_u and two B_{1u} are acoustic. Raman-active are the symmetric modes $7A_g + 5B_{1g} + 7B_{2g} + 5B_{3g}$, of which there are 24 in total.

Hexagonal $LuFeO_3$ possess a polar $P6_3cm$ structure with six formula units per unit cell with 38 Raman active phonon modes ($9A_1 + 14E_1 + 15E_2$), similar to hexagonal manganites of the same symmetry [4, 5]. For the scattering configuration used in our experiments (backscattering along the *z* direction parallel to the *c*-axis of *h*-$LuFeO_3$), modes of A_1 and E_2 symmetries are allowed in $z(x, x)\bar{z}$ geometry (parallel polarizations of incident and scattered light), while only E_2 modes are active in perpendicular polarization geometry $z(x, y)\bar{z}$.

The temperature evolution of the Raman spectra of the *h*-$LuFeO_3$ film over the range 10–1250 K is shown in Fig. S7. Spectra at elevated temperatures were measured in air in order to avoid decomposition of the films. Therefore, they contain multiple peaks in the low-frequency range (below 200 cm^{-1}), which are due to scattering by rotational excitations of molecules of air. The room temperature spectrum measured after heating up to 1250 K has the same shape and intensity as the spectrum before heating, thus indicating that no noticeable decomposition occurred during heating. The most noticeable change in the Raman spectra with increasing temperature is a decrease of relative intensity of the A_1 modes (the peaks seen in Fig. 1 near 296 and 657 cm^{-1}). The peak around 655 cm^{-1} is the strongest at low temperatures; its intensity is about 10 times higher compared to the E_2 modes at ~415 and 480 cm^{-1}. At high temperatures, the A_1 peak becomes as weak as those E_2 peaks (see Fig. S5-Right) showing enlarged high temperature spectra).

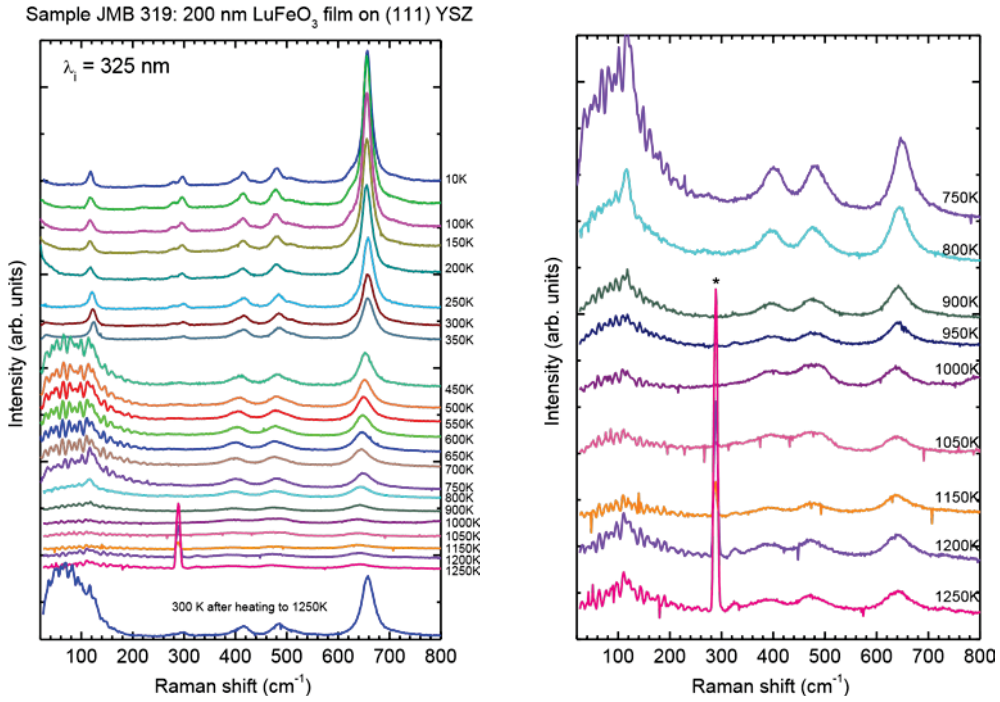

Fig. S7 (Left) Raman spectra of a YSZ-200 nm measured in parallel polarization configuration ((x, x)) as a function of temperature. **(Right)** Enlarged part of the left panel showing high temperature spectra. Sharp peak labeled by asterisk (*) is a thermally induced atomic emission line from the copper sample holder.

Piezoelectric Force Microscopy

Piezoelectric force microscopy (PFM) was performed to determine the ferroelectric polarizability of the *h*-$LuFeO_3$ in the polar state as determined by Raman spectroscopy. A single-crystal film of platinum was grown on top of YSZ substrate via DC magnetron sputter to act as a bottom electrode for PFM measurements; a 200 nm thick film of *h*-$LuFeO_3$ was then deposited on top of this platinum layer by MBE as previously described. The polarization parallel to the *c*-axis was examined at room temperature by poling the as-grown sample with a ±12 V bias. A 3 μm x 3 μm region was first poled using a -12 V bias such that the polarization points into the plane and shown in Fig. S6 as indicated by the lighter shaded region in the figure. The polarization of a 1 μm x 1 μm box within this poled region was then reversed by applying a voltage of +12 V, indicated as the darker region. This conclusively demonstrates that the material is ferroelectric at room temperature in agreement with Raman spectroscopy and previous measurements, and consistent with previous measurements of thin films fabricated with platinum buffer layers.

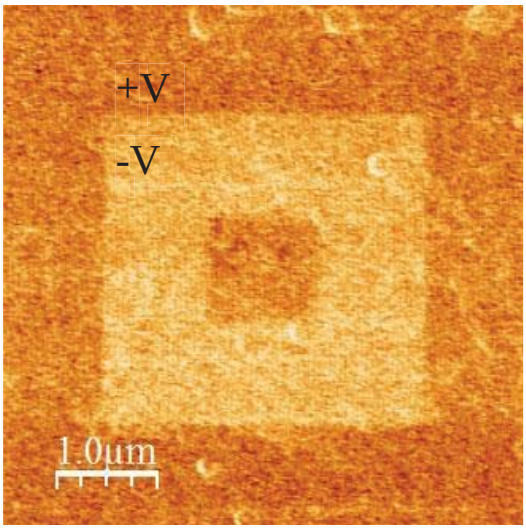

Fig. S8 An out-of-plane PFM image displaying a box-in-box structure that was written by poling the sample with ± 12V. Darker (lighter) regions correspond to a ferroelectric polarization out of (into) the plane.

Supplemental Material References

[1] W. Wang, J. Zhao, W. Wang, Z. Gai, N. Balke, M. Chi, H. N. Lee, W. Tian, L. Zhu, X. Cheng, D. J. Keavney, J. Yi, T. Z. Ward, P. C. Snijders, H. M. Christen, W. Wu, J. Shen, and X. Xu, Phys. Rev. Lett. **110**, 237601 (2013).

[2] J. A. Moyer, R. Misra, J. A. Mundy, C. M. Brooks, J. T. Heron, D. A. Muller, D. G. Schlom, and P. Schiffer, APL Mater. **2**, 012106 (2014).

[3] S. Venugopalan and M. M. Becker, J. Chem. Phys. **93**, 3833 (1990).

[4] M. N. Iliev, H. G. Lee, V. N. Popov, M. N. Abrashev, A. Hamed, R. Lmeng, and C. W. Chu, Phys. Rev. B **56**, 2488 (1997).

[5] A. Ghosh, J. R. Sahu, S. V. Bhat, and C. N. R. Rao, Solid State Sci. **11**, 1639 (2009).